Journal of Virology®

PATHOGENESIS AND IMMUNITY

Type I Interferon Receptor Signaling Drives Selective Permissiveness of Astrocytes and Microglia to Measles Virus during Brain Infection

Jeremy Charles Welsch,[a,b]* Benjamin Charvet,[a]* Sebastien Dussurgey,[c] Omran Allatif,[a] Noemie Aurine,[a] Branka Horvat,[a,b] Denis Gerlier,[a,b] Cyrille Mathieu[a,b]

[a]CIRI, International Center for Infectiology Research, CIRI, International Center for Infectiology Research, Inserm, U1111, Université Claude Bernard Lyon 1, CNRS, UMR5308, Ecole Normale Supérieure de Lyon, Université de Lyon, Lyon, France

[b]LabEx Ecofect, Université de Lyon, Lyon, France

[c]SFR BioSciences, INSERM, CNRS, UMS3444/US8, Ecole Normale Supérieure de Lyon, Université Claude Bernard Lyon 1, Lyon, France

ABSTRACT Fatal neurological syndromes can occur after measles virus (MeV) infection of the brain. The mechanisms controlling MeV spread within the central nervous system (CNS) remain poorly understood. We analyzed the role of type I interferon (IFN-I) receptor (IFNAR) signaling in the control of MeV infection in a murine model of brain infection. Using organotypic brain cultures (OBC) from wild-type and IFNAR-knockout ($IFNAR^{KO}$) transgenic mice ubiquitously expressing the human SLAM (CD150) receptor, the heterogeneity of the permissiveness of different CNS cell types to MeV infection was characterized. In the absence of IFNAR signaling, MeV propagated significantly better in explant slices. In OBC from IFNAR-competent mice, while astrocytes and microglia were infected on the day of explant preparation, they became refractory to infection with time, in contrast to neurons and oligodendrocytes, which remained permissive to infection. This selective loss of permissiveness to MeV infection was not observed in $IFNAR^{KO}$ mouse OBC. Accordingly, the development of astrogliosis related to the OBC procedure was exacerbated in the presence of IFNAR signaling. In the hippocampus, this astrogliosis was characterized by a change in the astrocyte phenotype and by an increase of IFN-I transcripts. A proteome analysis showed the upregulation of 84 out of 111 secreted proteins. In the absence of IFNAR, only 27 secreted proteins were upregulated, and none of these were associated with antiviral activities. Our results highlight the essential role of the IFN-I response in astrogliosis and in the permissiveness of astrocytes and microglia that could control MeV propagation throughout the CNS.

IMPORTANCE Measles virus (MeV) can infect the central nervous system (CNS), with dramatic consequences. The mechanisms controlling MeV invasion of the CNS remain ill-defined since most previous data were obtained from postmortem analysis. Here, we highlight for the first time the crucial role of the type I interferon (IFN-I) response not only in the control of CNS invasion but also in the early permissiveness of glial cells to measles virus infection.

KEYWORDS measles virus, astrogliosis, cell permissiveness, central nervous system infections, interferons, organotypic brain cultures

Measles virus (MeV) can infect neural cells and can cause lethal encephalitis and/or persistent brain infection that can lead to disease relapses from several months to years after primary infection. While studies have highlighted different mutations affecting the formation of infectious particles and their fusion machinery, in both cases, the mechanisms underlying early viral neuropathogenesis remain ill defined (1–6).

Citation Welsch JC, Charvet B, Dussurgey S, Allatif O, Aurine N, Horvat B, Gerlier D, Mathieu C. 2019. Type I interferon receptor signaling drives selective permissiveness of astrocytes and microglia to measles virus during brain infection. J Virol 93:e00618-19. https://doi.org/10.1128/JVI.00618-19.

Editor Rebecca Ellis Dutch, University of Kentucky College of Medicine

Address correspondence to Jeremy Charles Welsch, jrmy.welsch@gmail.com, or Cyrille Mathieu, cyrille.mathieu@inserm.fr.

* Present address: Jeremy Charles Welsch, University of Michigan, Ann Arbor, Michigan, USA; Benjamin Charvet, GeNeuro, Geneva, Switzerland.

Received 13 April 2019
Accepted 16 April 2019
Accepted manuscript posted online 24 April 2019
Published 14 June 2019

MeV first invades the immune system by infecting activated SLAM (CD150)-expressing immune cells. Secondarily, MeV infects epithelia from the basolateral side by using Nectin-4 to egress from the host respiratory tract and to enable human-to-human dissemination (7–9). MeV can also reach the central nervous system (CNS), leading to a rare but serious neurological syndrome that can affect people within days to years after the acute phase of the infection and that often results in severe disability and death (10–12). CNS infections are often accompanied by demyelination and are associated with lesions of the cerebral cortex, the hippocampus, the thalamus, the brain stem, and, to a lower extent, the cerebellar cortex (13, 14). Viral proteins are always immunodetected in neurons, oligodendrocytes, and, much less frequently, astrocytes or microglia (10, 15, 16). The present knowledge of MeV CNS invasion is limited to that obtained by clinical examination, serology, postmortem viral isolation, RNA sequencing, and tissue immunostaining.

Type I interferon (IFN-I) plays an important role in the control of infections by viruses (17). Transgenic mouse models expressing a human receptor allowing MeV entry have been instrumental for studying both the key role of IFN-I receptor (IFNAR) signaling and MeV invasion of the CNS (18–21). In particular, intranasal (i.n.) MeV infection of suckling mice ubiquitously expressing the human SLAM transgene causes virus invasion of the central nervous system, leading to a lethal acute neurological syndrome (21). This pathology is exacerbated when combined with an IFNAR deficiency, leading to a lethal neurological syndrome and confirming the crucial global role of IFN-I signaling in the control of MeV infection *in vivo* (21, 22). The current work aimed at furthering our cellular and molecular insights into the mechanisms underlying the role of IFN-I in MeV infection of the CNS. The kinetics of MeV propagation within the hippocampus were investigated in organotypic brain cultures (OBC) (23–25) from SLAM and SLAM $\times$ IFNAR-knockout (IFNAR^{KO}) transgenic (tg) mice. The data obtained highlight the crucial role of IFN-I signaling in the selective cellular permissiveness to infection.

RESULTS

A lack of IFN-I signaling significantly enhances MeV infection and dissemination in the hippocampus. Since the hippocampus is one of the targets of MeV in the central nervous system, we have focused on this substructure to better understand the early steps of its viral invasion (13, 14, 26). After infection of OBC from SLAM tg mice on the day of slice preparation, enhanced green fluorescent protein (EGFP)-tagged MeV (MeV-EGFP) progressively disseminated through the entire explant (Fig. 1A), as previously observed (23–25). The most efficient viral propagation occurred when the infection was performed on the same day as slice preparation (day 0), as determined by quantifying MeV N RNA by reverse transcription-quantitative PCR (RT-qPCR) (Fig. 1B). Delaying MeV infection resulted in a significant decrease in viral RNA accumulation at 3 days postinfection (dpi), reaching up to a 100-fold reduction after 7 days of culture.

When SLAM $\times$ IFNAR^{KO} OBC were infected, the IFN-I receptor deficiency facilitated MeV replication, as revealed by the significant 2.5-fold increase of accumulated N RNA at 3 dpi when the virus was applied at day 0 (Fig. 1B). This increase in MeV replication was even more pronounced when the infection was performed after 7 days of culture, with a 15-fold increase in N RNA accumulation. However, as observed with SLAM tg mouse OBC, the amount of MeV N RNA that accumulated over 3 days of infection progressively decreased with the delay of the infection. These data highlight the ability of the IFN-I system to control the initial susceptibility of the hippocampus to the infection. Furthermore, they suggest that the injury caused by the slicing and *ex vivo* culture triggers a response related to IFN-I that dramatically decreases the ability of this structure to support MeV replication and dissemination.

Interferon response in OBC. The effect of the slicing procedure on the activation of IFN-I was then investigated in hippocampal slices by measuring alpha interferon (IFN-α) and IFN-β mRNA over 7 days of culture in the absence of MeV infection. In both tg mouse OBC, the levels of the tested IFN-α subtype transcripts (i.e., subtypes 1, 5, 6, 7, 12, 14, 15, 16, and, to a lower extent, 9 and 13) did not significantly vary over time

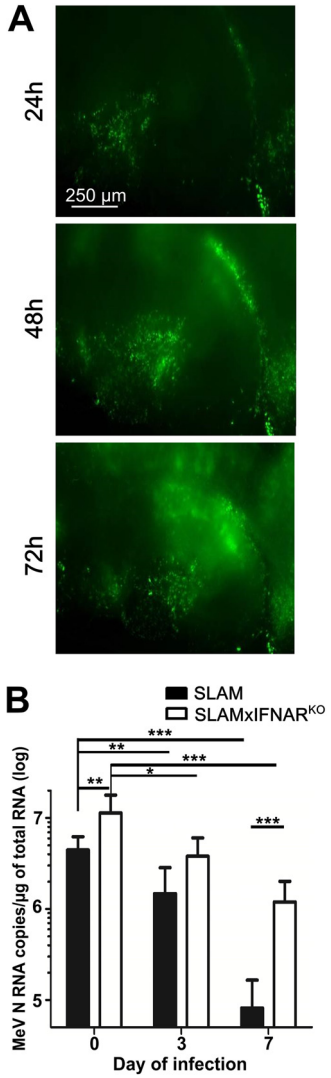

FIG 1 Increased MeV replication in OBC in the absence of IFNAR signaling. (A) MeV IC323-EGFP dissemination in hippocampus slices from SLAM tg mice infected on the day of culture with 10,000 PFU, followed by fluorescence imaging over 72 h. Pictures were reconstituted using the MosaicJ plug-in with ImageJ software. (B) Amounts of viral nucleoprotein RNA copies accumulated over 3 days in hippocampus slices ($n = 5$) from SLAM and SLAM $\times$ IFNAR^{KO} mice infected with 10,000 PFU of MeV at day 0, 3, and 7 of *ex vivo* explant culture. MeV N RNA was quantified by RT-qPCR and normalized to the standard deviation for GAPDH mRNA. Statistical analyses were performed using the Mann-Whitney U test. *, $P < 0.05$; **, $P < 0.01$; ***, $P < 0.001$.

(Fig. 2A). IFN-β mRNA remained stable in SLAM tg OBC from day 0 to day 3 and was higher than that observed in SLAM $\times$ IFNAR^{KO} hippocampus slices. At day 7 of culture, corresponding to the time when the slices displayed the lowest permissiveness to viral infection (Fig. 1B), the difference became significant, with ~6-fold and ~16-fold increases in slices from SLAM and SLAM $\times$ IFNAR^{KO} mice, respectively (Fig. 2B). As a proof for the deficiency of IFNAR signaling in SLAM $\times$ IFNAR^{KO} explants, the levels of MX1 mRNA were found to remain invariant throughout the tissue culture, contrary to the findings for the SLAM tg mouse hippocampi, where its induction was already significant after 1 day (Fig. 2C). This result also suggests that other IFN-α subtype transcripts, such as those of IFN-α subtype 4, may be induced earlier in SLAM tg OBC.

Development of astrogliosis in OBC. OBC preparation is a stressful process which inherently disrupts the tissue, alters its homeostasis, and quickly leads to cell loss before recovery (25). Astrocytes are known to play an important role in CNS healing in

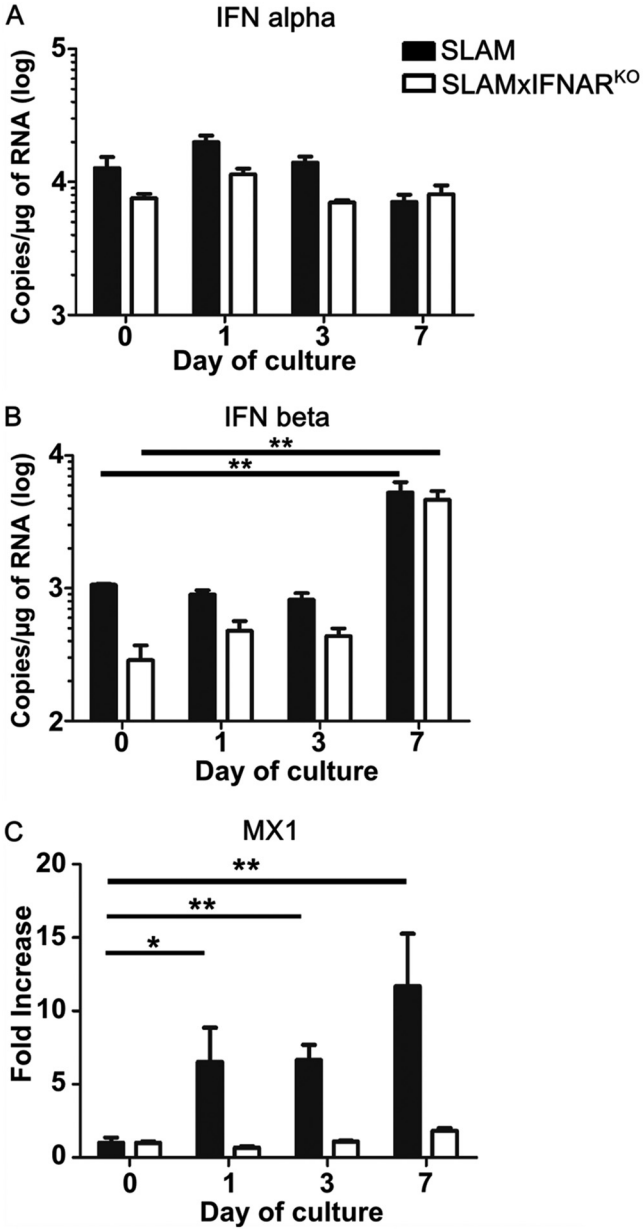

FIG 2 Interferon mRNA expression in hippocampus explants. The levels of IFN-α (A), IFN-β (B), and MX1 (C) mRNA were quantified over time in slices from SLAM transgenic mice ($n = 7$), and SLAM $\times$ IFNAR^{KO} transgenic mice ($n = 5$) at days 0, 3 and 7 of culture. All RNA quantifications were done by RT-qPCR and normalized to the variation of the amounts of GAPDH mRNA. Statistical analyses were performed using the Kruskal-Wallis test. *, $P < 0.05$; **, $P < 0.01$.

response to brain injuries (27–29). Thus, their distribution, behavior, and morphology were analyzed over the 7 days of culture by immunostaining.

After 7 days of culture and GFAP (glial fibrillary-associated protein) immunostaining, hippocampal OBC from either SLAM or SLAM $\times$ IFNAR^{KO} mice exhibited a cellular hypertrophy and a partial loss of individual astrocyte domains with visible overlapping processes, a feature that is typical of severe diffuse astrogliosis (Fig. 3A) (30). Since the GFAP staining of slices from both mouse models looked almost undistinguishable, the kinetics of the accumulation of GFAP and S100B mRNA, two markers of activation and global cell activation, respectively, were analyzed by RT-qPCR. GFAP mRNA was found to be upregulated in the hippocampus slices from SLAM tg mice with a significant 26-fold increase that peaked after 3 days of culture and that slightly decreased at day

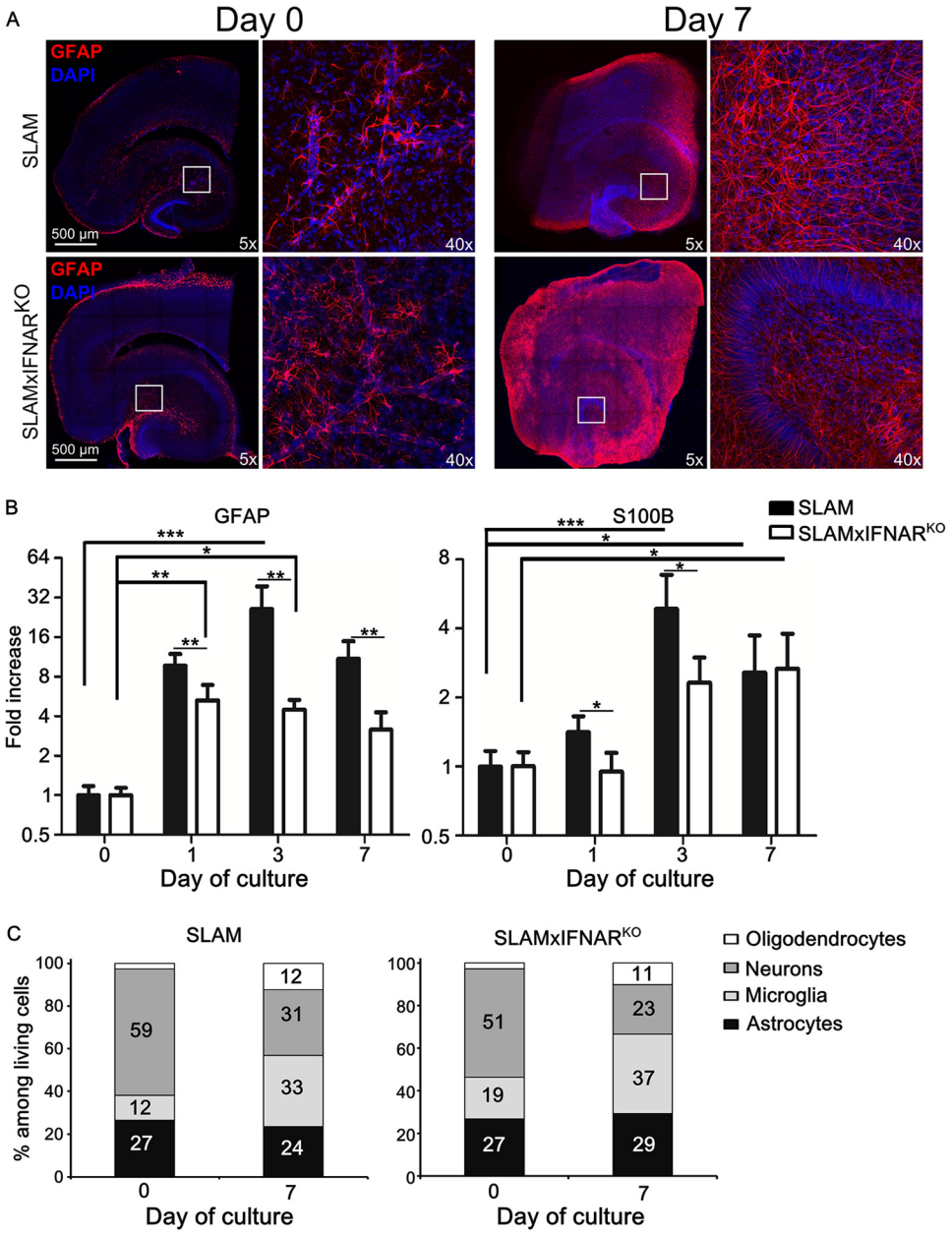

FIG 3 Astrogliosis and cellular activation during *ex vivo* hippocampal explant culture. (A) SLAM and SLAM × IFNAR^{KO} mouse hippocampus slices (at least 5 slices/animal) were stained with anti-GFAP antibody (an astrocyte marker). Nuclei were counterstained with DAPI. Images were taken at the indicated time of culture with a Leica SP5 confocal microscope and show a high level of activation of astrocyte populations at a low magnification (reconstructed tile; left) or a high magnification (×40 objective; right) in response to slicing and culture procedures. (B) Monitoring of GFAP (an astrocyte proliferation marker) and S100B (a global activation marker) mRNA expression in SLAM and SLAM × IFNAR^{KO} mouse hippocampus OBC ($n = 5$) during the first week of culture by RT-qPCR (normalized to the standard deviation for GAPDH mRNA). The results are presented as the fold increase in expression compared to that on day 0. Statistical analyses were performed using the Kruskal-Wallis test. *, $P < 0.05$; **, $P < 0.01$; ***, $P < 0.001$). (C) The evolution of cell composition over 7 days of culture was studied by flow cytometry both in SLAM and in SLAM × IFNAR^{KO} mouse hippocampus OBC ($n = 3$). The results are presented as the percentage of stained cells among living cells after OBC dissociation.

7. In slices from SLAM × IFNAR^{KO} mice, GFAP mRNA also increased with time, but it peaked earlier, at day 1 (5.3-fold), remained significant at day 3 (4.5-fold), and slightly decreased at day 7. This increase of GFAP transcription was significantly lower than that observed in hippocampus slices from SLAM mice throughout the 7-day postculture period. The kinetics of the accumulation of S100B mRNA paralleled those observed for

GFAP transcripts, with a significant 4.9-fold overexpression after 3 days in the SLAM hippocampus that remained elevated thereafter (2.7-fold). Similarly, in the SLAM × IFNAR^{KO} background, S100B mRNA upregulation was slower and progressively reached a significant 2.7-fold increase only after 7 days. As observed for GFAP, the overall increase in the accumulated S100B transcripts was significantly higher in SLAM tg OBC than in SLAM × IFNAR^{KO} OBC at day 1 and day 3, before ending at a similar level, confirming the slower response in the IFN-I receptor-deficient model. This suggests that the activation of the astrocytes is reinforced in the presence of the IFN-I system (Fig. 3B). We followed the cell composition of OBC from both models over 1 week by flow cytometry (Fig. 3C). As expected, the 4 cell populations remained represented over 7 days. As previously observed, the slicing procedure led to a loss of neurons, with 23% to 30% of the cells surviving the dissociation/staining protocol after 1 week of culture. The astrocyte population seemed to be constantly maintained, as observed in moderate astrogliosis (30). Oligodendrocyte and microglial proportions were multiplied by 2 to 3 times after 7 days, potentially either because of the differentiation of precursors or because their morphology allowed better survival from the dissociation procedure prior to flow cytometry.

Analysis of production of cytokines during astrogliosis in hippocampus OBC. The global cellular activation and tissue remodeling during the *ex vivo* culture were further analyzed by quantifying a set of secreted proteins related to inflammation and astrogliosis in OBC from SLAM tg and SLAM × IFNAR^{KO} mice at days 0 and 7 by using a proteomic analysis assay (Fig. 4). For each type of mouse, two consecutive hippocampus slices were isolated from 4 animals, with one being used for proteome analysis at day 0 and the other being used for analysis after 7 days of *ex vivo* culture (Fig. 4A).

In SLAM tg mouse OBC, box plots showed a significant increase of 84/111 proteins in each of the 4 tested individuals ($P < 0.001$, linear mixed-model regression analysis) (Fig. 4B and C and Fig. 5). The upregulation concerned 25/31 cytokines, 21/22 chemokines, 13/14 growth factors, and 25/44 other unclassified proteins (Fig. 4C and 5). Among the 24 known referenced markers of astrogliosis that were included in the array, 18 of them were significantly overexpressed after 7 days. Seven cytokines (interleukin-1β [IL-1β], IL-28, IL-33, IL-7, IL-23, tumor necrosis factor alpha [TNF-α], and IFN-γ) known to be involved in antiviral activity were significantly overexpressed (Fig. 5, arrows). Thus, as expected, the slice preparation and culture procedures also led to an inflammatory status of the *ex vivo* hippocampus explant. In hippocampus explants from SLAM × IFNAR^{KO} mice, only 27 proteins (Fig. 4B), including 6 cytokines, 6 chemokines, 7 growth factors, and 8 unclassified proteins (Fig. 4C and 5), were significantly upregulated after 7 days of culture ($P < 0.001$, linear mixed-model regression analysis). As expected from the lower levels of GFAP and S100B mRNA accumulation, only 7 proteins belonged to referenced markers of astrogliosis. Six of them were also upregulated in SLAM mice, and the protease matrix metalloproteinase 3 (MMP3) was uniquely upregulated in the SLAM × IFNAR^{KO} hippocampus (Fig. 4C and 5). None of the few cytokines overexpressed in the SLAM × IFNAR^{KO} hippocampus is known to exhibit antiviral properties.

Finally, a two-way analysis of variance (ANOVA) was performed to ascertain whether the evolution of protein expression patterns over the week of culture was different between SLAM and SLAM × IFNAR^{KO} OBC. Not only did the secretory proteome significantly vary with the length of tissue culture ($P < 0.001$), but there was also a significant relation between the length of tissue culture and the mouse model studied ($P < 0.001$), meaning that the reactivity varied according to the presence or absence of the IFNAR functional pathway. Indeed, in agreement with the observations presented above, the hippocampus from SLAM mice was significantly more reactive to the slicing procedure and culture than its SLAM × IFNAR^{KO} model counterpart.

The effect of MeV infection on the secreted proteome was evaluated by comparing the proteome of explants infected or not on the day of their preparation (day 0) and that of explants harvested 3 days later, corresponding to a total of 3 days of culture (Fig. 6). The level of infection after 3 days was similar in all infected SLAM slices (Fig. 6A). Infection was associated with a significant modification of the global protein expression

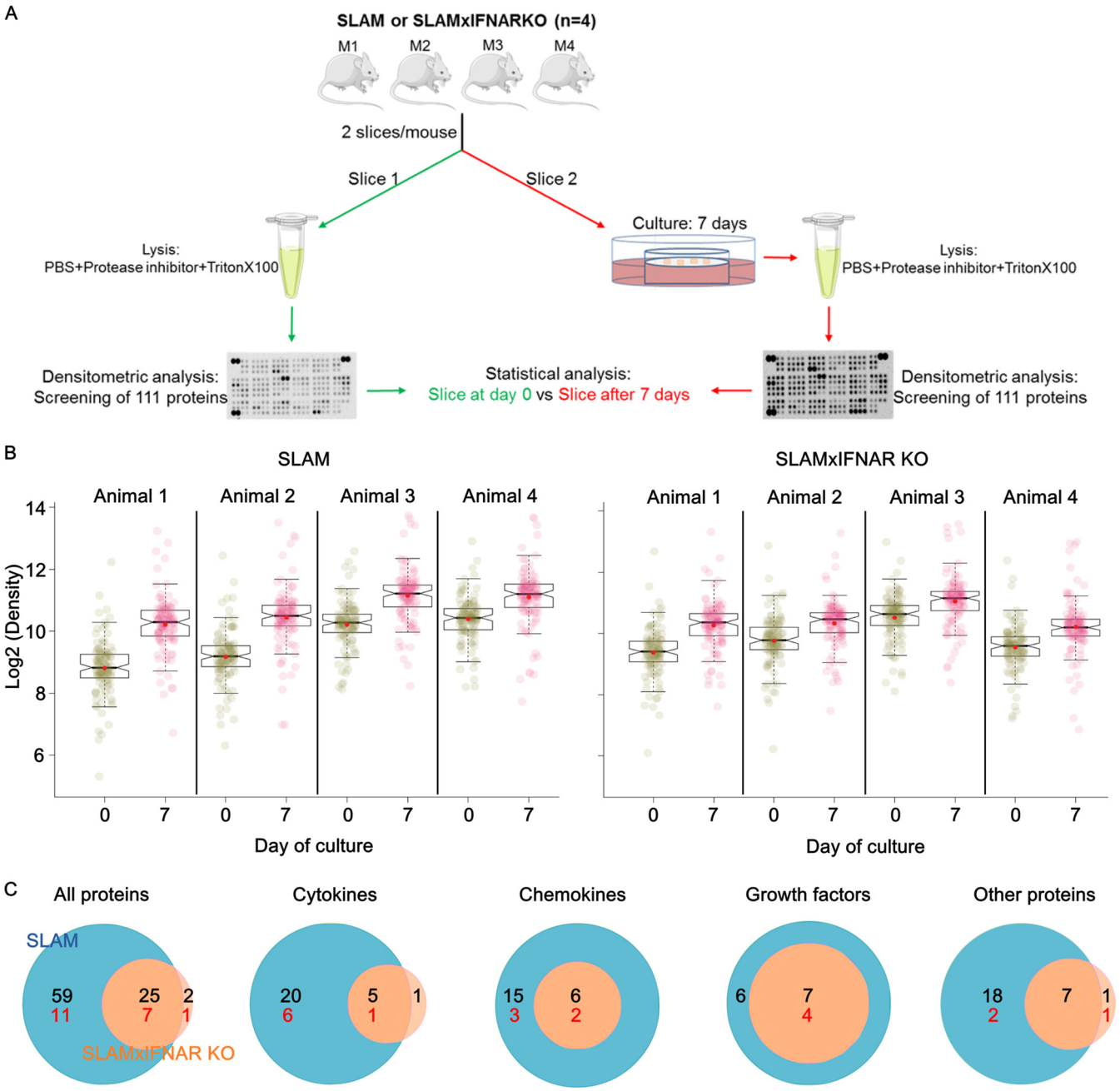

FIG 4 Global overview of the proteomic analysis of SLAM and SLAM × IFNAR^{KO} mouse OBC over 7 days of culture. (A) Schematic overview of the experiment. The SERVIER Medical Art image bank (Creative Commons 3.0; https://creativecommons.org/licenses/by/3.0/) helped to create this image. (B) Box plots show the expression range and individual values for the 111 secreted proteins included in the proteome array ($n = 4$). The notches in the box plots represent the median 95% confidence intervals, and red dots represent the expression average. The closeness between the mean and median values argues for a Gaussian distribution for protein production. (C) Venn diagrams account for statistically significant proteins that are either common to both mouse strains or specific to each mouse strain and clustered in 4 main protein classes. The numbers of proteins so far considered markers of astrogliosis are shown in red.

pattern ($P < 0.001$, linear mixed-model regression analysis) (Fig. 6B). Fifty out of the 111 tested proteins were significantly overexpressed in the infected slices (Table 1) (fold change in expression ≥ 1.7, adjusted $P < 0.05$), with 13 of them being increased by more than 2-fold. Five of the latter were cytokines and chemokines that are associated with the inflammasome and NF-κB pathways and that are generally observed in the initiation of an immune response to any virus infection (i.e., IL-1β, CCL5, CXCL10, CCL19, CCL17). Two of the most overexpressed interleukins (IL-2 and IL-10) were previously reported to be induced in peripheral immune cells infected with MeV. Importantly, the

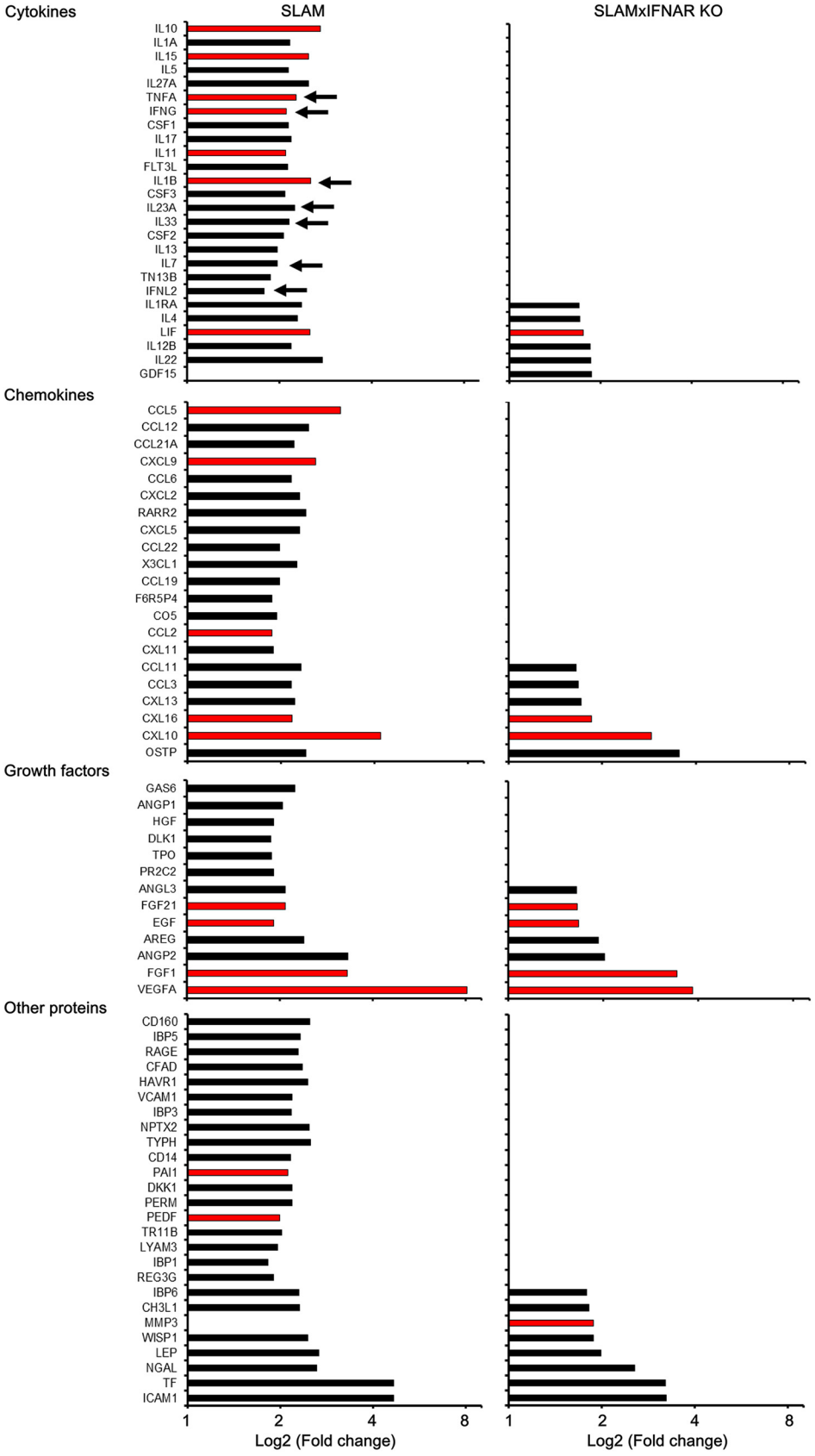

FIG 5 Proteomic analysis of SLAM and SLAM × IFNAR^{KO} mouse OBC over 7 days of culture. This graphic displays only the proteins that showed a statistically significant difference in their expression between day 0 and day 7.

(Continued on next page)

44 out of 50 proteins upregulated upon MeV infection also belong to the set of proteins upregulated because of the astrogliosis response to the slicing and culture procedure. In other words, MeV infection exacerbated the type I IFN-dependent astrogliosis response. Several growth factors were also upregulated, but most of them have not yet been reported to be associated with MeV infection. Surprisingly, platelet-derived growth factor B (PDGF-BB) was among the most overexpressed proteins and was expressed only after infection. This protein has been associated with simian human immunodeficiency virus encephalitis (31). The expression of the Tat protein from this virus in astrocytes has also been shown to induce the overexpression of PDGF-BB, leading to increased astrogliosis and proinflammatory responses in the brains of HIV-infected individuals (32). Matrix metalloproteinase 9 (MMP9) was also among the 13 most overexpressed proteins and was overexpressed only in the infectious context (Table 1). This protein, reflecting brain damage, was already observed in cerebrospinal fluids from subacute sclerosing panencephalitis patients (33). It may play an important role in the development of MeV-related encephalitis, as observed in a model of experimental autoimmune encephalomyelitis, by affecting the blood-brain barrier integrity (34). Moreover, while it has never before been highlighted for MeV, this protein is known to bind type I IFN receptor, inhibiting the downstream JAK/STAT signaling and thus facilitating replication for some other viruses, such as hepatitis B virus (35).

On the contrary, we did not observe any significant variation in the global secreted protein expression pattern when analyzing the secreted proteins that we detected in SLAM $\times$ IFNAR^{KO} infected hippocampi versus noninfected slices after 3 days (Fig. 6C). Only 5 proteins (i.e., CCL12, CSF2, IL-1β, CXCL5, CH3L1) tended to decrease, but not significantly, in infected slices (data not shown). This result confirms the incapacity of this model not only to trigger the antiviral response but also to initiate an appropriate astrogliosis/inflammatory pattern in response to the infection with MeV. To go further, the different patterns of secreted proteins between the two murine models in response to MeV infection suggest that the SLAM and SLAM $\times$ IFNAR^{KO} mice may develop encephalitis in a totally different way.

Analysis of hippocampus cell subtype susceptibility to MeV infection. The lower infection rate of IFN-competent OBC may be related to the lower susceptibility of specific cell types in the CNS. Thus, the permissiveness of each cell type of SLAM and SLAM $\times$ IFNAR^{KO} mouse OBC was first assessed after infection on the day of slicing (day 0). From confocal microscopy analyses, some neurons, oligodendrocytes, astrocytes, and microglia were found to be infected at 1 dpi (data not shown). This was expected, owing to the ubiquitous and quite homogeneous expression of the human SLAM cellular receptor (21), and was further confirmed by RT-qPCR measurements of each of these cell subsets after their sorting by flow cytometry (data not shown). The permissiveness of each cell subset to MeV-EGFP was further estimated by flow cytometry after gentle dissociation of the hippocampus slices into a single-cell suspension (Fig. 7A and B). Surface markers for microglia (CD11b) and oligodendrocytes (GalC) versus intracellular markers after fixation/permeabilization staining for astrocytes (GFAP) and neurons (Tuj1 [beta III tubulin]) for internal markers had to be used for technical reasons. Despite the ubiquitous expression of the receptor, in the SLAM model, neurons exhibited the highest proportion of EGFP staining. Indeed, the analysis of the distribution of MeV infection showed EGFP in up to 60% of neurons, 25% of astrocytes, and less than 5% of oligodendrocytes and microglia (Fig. 7C). The proportions of infected neurons in the

FIG 5 Legend (Continued)
The proteins here are ordered by increasing $\log_2$ fold change in expression observed in SLAM $\times$ IFNAR^{KO} mouse OBC and are grouped by protein class; day 0 is the reference time point. Red bars indicate proteins related to astrogliosis. Arrows indicate genes known to be involved in antiviral effects. Proteins differentially expressed between day 0 and day 7 were determined with the linear model approach from the Bioconductor limma package. Analyses were completed for each mouse strain separately ($n = 4$ mice at each time point). Data were paired by animal, and P values were corrected for multiple testing with the Bonferroni adjustment method. A difference was considered significant when the adjusted P value was <0.05.

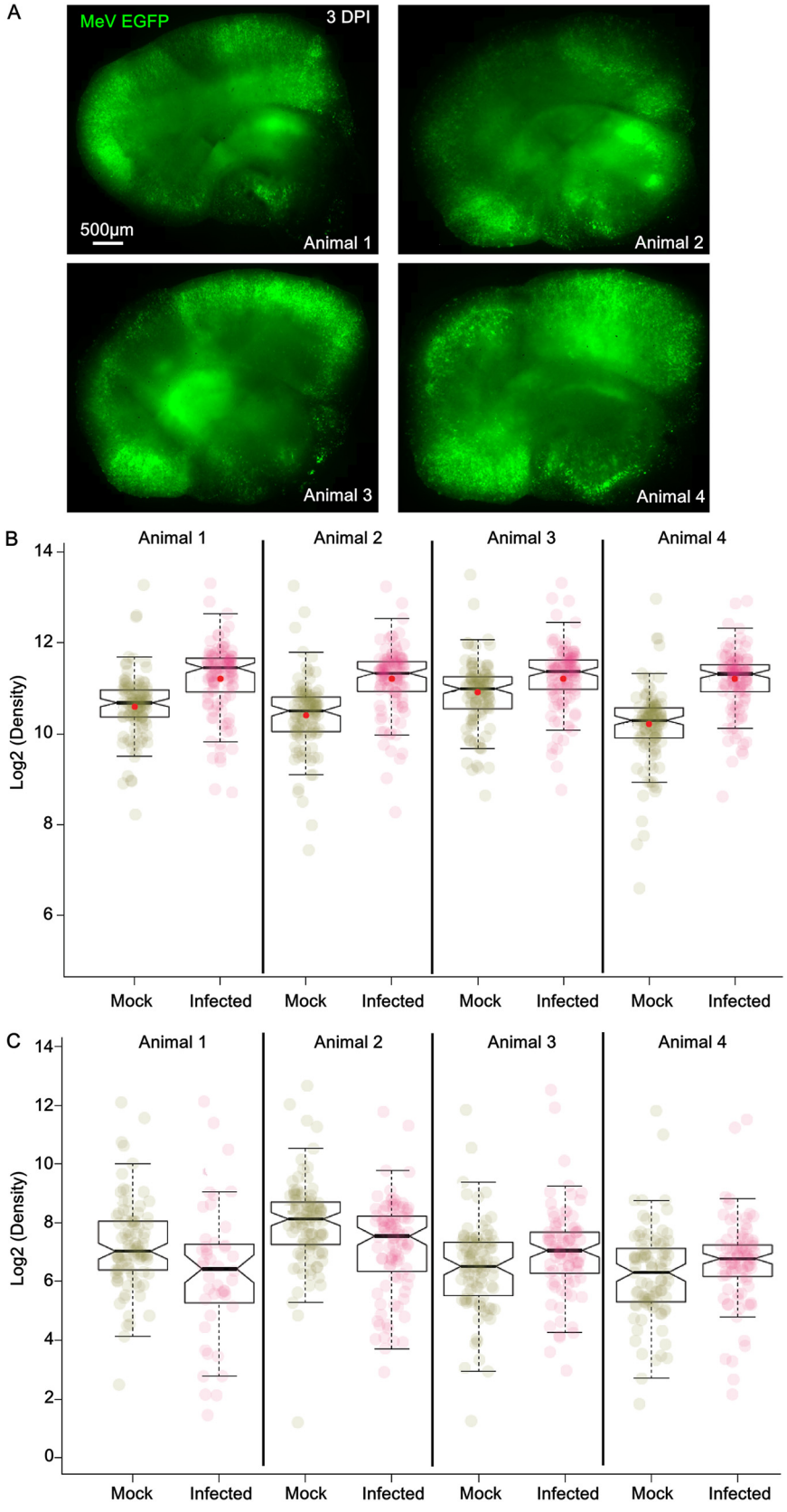

FIG 6 Global overview of the infection effect on the proteomic profile of OBC after 3 days of culture. (A) Mosaic reconstitution of hippocampal slices from 4 different SLAM mice at 3 days postinfection with 10^4 PFU of MeV IC323-EGFP (in green), observed using an inverted fluorescence microscope (Zeiss) and

(Continued on next page)

SLAM × IFNAR^{KO} mouse hippocampal slices decreased below 40%. The percentage of infected oligodendrocytes slightly increased, while both infected astrocytes and microglia were detected in much greater proportions in the SLAM × IFNAR^{KO} slices than in their SLAM counterparts (i.e., 35% of astrocytes and 20% of microglia) (Fig. 7C). This suggests that the IFNAR defect selectively renders the last two cell populations more permissive to MeV infection. To go further, the contribution of each cell type to the infection was analyzed by evaluating the percentage of infected cells among each stained cell population that was still alive after the dissociation of the tissue (Fig. 7D). In SLAM OBC, neurons remained the main contributors to infection, with 2.8% of the stained cells being infected, followed by oligodendrocytes (1.8% of infected cells), while microglia and astrocytes seemed to contribute less to the infection (i.e., 1.21 and 1.25% infected cells). In SLAM × IFNAR^{KO} mouse OBC, the percentage of infected cells among neurons decreased to 1.46%, while it increased to 1.5% for the astrocytes. This increase was even more significant for microglia and oligodendrocytes, among which the percentage of infected cells increased to 3.5 and 7.6%, respectively (Fig. 7D). These results suggest that in IFN-competent OBC, neurons are not only the most represented infected cells but also the main contributors to the early infection. On the contrary, in the absence of IFNAR, astrocytes are at least as permissive as neurons, while microglia and oligodendrocytes become the main contributors to the early events of infection.

When MeV infection of SLAM OBC was performed after 7 days of culture, neurons and oligodendrocytes remained similarly permissive to MeV (data not shown), while none of the astrocytes and microglial cells could be found to be infected at 1 dpi (Fig. 8A and C), as if they had become totally refractory to infection. The astrocytes and microglia of the hippocampus slices from SLAM × IFNAR^{KO} mice were infected even when the infection was delayed up to 7 days after the start of *ex vivo* culture (Fig. 8B and D).

Overall, the data indicate that IFN-I can play a major role in controlling the susceptibility of oligodendrocytes, microglia, and astrocytes to MeV infection in a manner that is independent of receptor expression and that is predictive of the efficiency of viral dissemination throughout the hippocampus in this experimental model.

DISCUSSION

To date the ability of MeV to disseminate through the hippocampal neuronal network has been addressed in mice and rats (36–38), but the restriction to neurons and oligodendrocytes as well as the exclusion of dissemination to astrocytes and microglia remains largely unexplored. Contrary to other encephalitic paramyxoviruses, such as canine distemper virus, that infect and disseminate throughout the astrocyte network (39), MeV preferentially targets neurons in the early step of CNS infection even in the presence of the artificial ubiquitous expression of human SLAM (Fig. 7). The lower permissiveness of glial cells to MeV infection may lead to their activation and, thus, the acquisition of a resistant phenotype of astrocytes and microglia. Here, we notably show that this resistance passes by the acquisition of a reactive phenotype directly related to the type I IFN signaling pathway (Fig. 3, 7, and 8). Unexpectedly, neurons did not

FIG 6 Legend (Continued)
camera (AxioCam; Zeiss). (B) Box plots show the expression range and individual values for the secreted proteins included in the proteome array after 3 days of culture of OBC from SLAM mice ($n = 4$). Under the infected condition, slices received 10^4 PFU of MeV IC323-EGFP at day 0, while under the mock-infected condition, the slices received an equivalent amount of medium. Notches in the box plots represent the median 95% confidence intervals, and red dots represent the expression average. The closeness of the mean and median values argues for a Gaussian distribution for protein production. (C) Box plots show the expression range and individual values for the expressed secreted proteins included in the proteome array after 3 days of culture of OBC from SLAM × IFNAR^{KO} mice ($n = 4$). Under the infected condition, slices received 10^4 PFU of MeV IC323-EGFP at day 0, while under the mock-infected condition, the slices received an equivalent amount of medium. Notches in the box plots represent the median 95% confidence intervals, and red dots represent the expression average. The closeness of the mean and median values argues for a Gaussian distribution for protein production.

TABLE 1 Proteins oversecreted upon infection with MeV[a]

Protein	Adjusted *P* value	Fold change in expression
CXL10	5.73E−06	2.9
CCL5	1.24E−04	2.5
NGAL	7.21E−05	2.3
CFAD	5.47E−04	2.2
CRP	4.48E−02	2.2
IL1B	7.26E−04	2.1
PDGF-BB	1.35E−03	2.0
AREG	1.51E−03	2.0
CH3L1	2.87E−03	2.0
CCL19	2.14E−03	2.0
IL2	1.28E−02	2.0
F6R5P4/CCL17	2.89E−03	2.0
MMP9	1.55E−02	2.0
TN13B	1.95E−03	1.9
CXL16	6.09E−03	1.9
ANGL3	4.45E−03	1.9
FLT3L	3.89E−03	1.9
CO5	3.06E−03	1.9
IL10	4.60E−03	1.9
GDF15	7.94E−03	1.9
IL23A	5.53E−03	1.9
IL15	8.40E−03	1.9
FGF21	1.54E−02	1.9
CCL11	1.14E−02	1.9
CCL22	8.76E−03	1.9
TNFA	1.95E−02	1.9
IL12B	8.35E−03	1.8
DKK1	8.70E−03	1.8
IBP6	1.21E−02	1.8
PCSK9	3.06E−02	1.8
CCL12	8.15E−03	1.8
ADIPO	4.26E−02	1.8
WISP1	3.49E−02	1.8
CXL11	1.46E−02	1.8
CXCL9	2.65E−02	1.8
PERM	1.58E−02	1.8
IL11	4.66E−02	1.8
CC21A	1.88E−02	1.7
EGF	3.42E−02	1.7
IL1RA	2.33E−02	1.7
IL22	3.59E−02	1.7
CXL13	2.01E−02	1.7
CD14	2.05E−02	1.7
CXCL5	3.42E−02	1.7
ANGP1	2.13E−02	1.7
HAVR1	4.77E−02	1.7
ANGP2	1.96E−02	1.7
X3CL1	1.92E−02	1.7
FETUA	2.74E−02	1.7
IL13	4.32E−02	1.7

[a]Slices were infected or not at day 0, and the proteome analysis was done at day 3. The last column quotes the fold change in expression in MeV-infected slices over that in sham-infected ones.

develop any specific resistance to MeV infection related to IFNAR signaling, as previously observed in cultures of primary neurons from the hippocampus, where homeostatic IFN levels would participate in the early control of MeV infection (40).

Astrogliosis and microgliosis are commonly observed during MeV acute encephalitis (21, 41, 42). Our results agree with observations made by other groups with NSE-CD46 mice (42) showing that infection with MeV also leads to the overexpression of proinflammatory cytokines. Nevertheless, while similar to the cytokine profile that we observed in response to the slicing procedure to initiate the healing of the tissue, the response to the virus infection was significantly stronger and may explain the overrecruitment of lymphocytes in the CNS of patients developing MeV encephalitis (42).

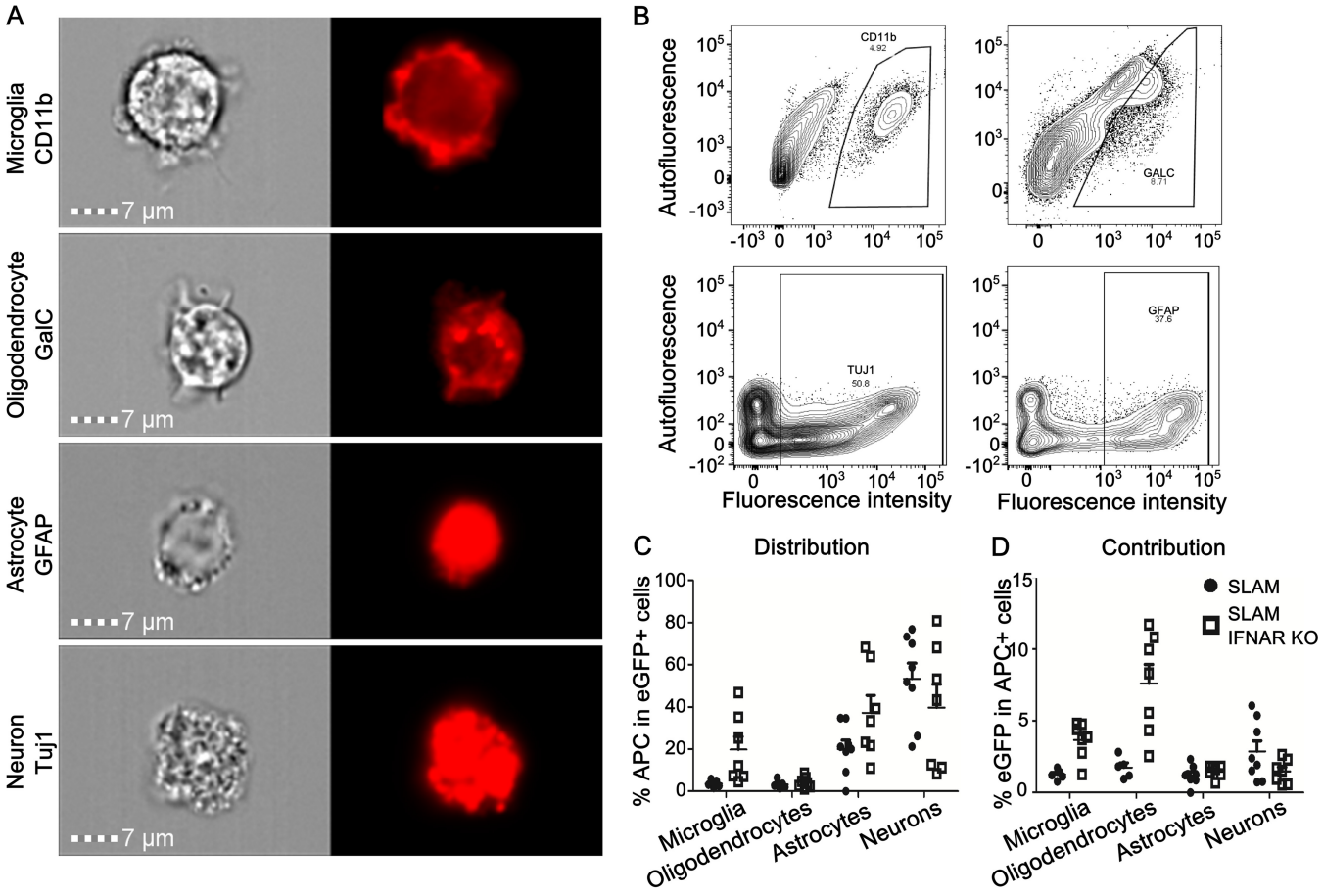

FIG 7 Flow cytometry analysis of cell permissiveness to MeV infection in hippocampus slices. (A) Validation of CNS cell staining using an ImageStreamX Mark II imaging flow cytometer. Microglia, oligodendrocytes, neurons, and astrocytes were stained using anti-CD11b, anti-GalC, anti-Tuj1, and anti-GFAP markers, respectively. (B) Graphical representation of the staining of microglia, oligodendrocytes, neurons, and astrocytes stained using respectively anti-CD11b, anti-GalC, anti-Tuj1, and anti-GFAP markers. (C) Quantification of SLAM and SLAM × IFNAR^{KO} OBC cell susceptibility to MeV infection by flow cytometry. Slices of hippocampus from either SLAM or SLAM × IFNAR^{KO} mice were infected with 2×10^4 PFU of MeV IC323-EGFP. After 24 h, slices were digested and cells were dissociated and stained for flow cytometry analyses. Microglia, oligodendrocytes, astrocytes, and neurons were stained using, respectively, anti-CD11b, anti-GalC, anti-GFAP, and anti-Tuj1 markers. The distribution of infection is represented as the percentage of each cell type within the subset of green fluorescent protein (GFP)-positive (infected) cells. (D) The contribution of each cell type to overall infection is shown as the percentage of GFP-expressing cells within the immunostained (APC-positive) cell subset for each condition ($n = 5$ to 7).

Previous studies showed that astrocytosis also takes place in animals lacking IFN signaling (42, 43). Here we also observed that astrocytes acquired an activated phenotype in SLAM × IFNAR^{KO} mouse explants (Fig. 3), but we clearly demonstrated that the secreted protein fingerprint was significantly different from that seen in the IFNAR-competent model (Fig. 4 and 5). The astrogliosis molecular signature in the SLAM × IFNAR^{KO} OBC was significantly less pronounced, despite a comparable change of morphology of the astrocyte population observed by imaging. Indeed, only a limited subset of secreted proteins was activated, indicating that the fully functional interferon pathway contributes at least quantitatively to the inflammatory response during astrogliosis. That an antiviral astrogliosis process appears to be dependent on an intact IFN-I response has not yet been reported, to the best of our knowledge. The 27 secreted proteins (including 8 cytokines) that are upregulated in the absence of IFNAR signaling may represent the basal astrogliosis response required to start the process of healing of the CNS following a physical injury. Whether this intrinsic response is responsible for the significant, albeit small, decrease in the susceptibility of SLAM × IFNAR^{KO} OBC maintained in culture for several days before MeV infection or whether this small loss in susceptibility resulted from the loss of major targets or cellular rearrangement occurring during the culture procedure (25) will need further investigation. For exam-

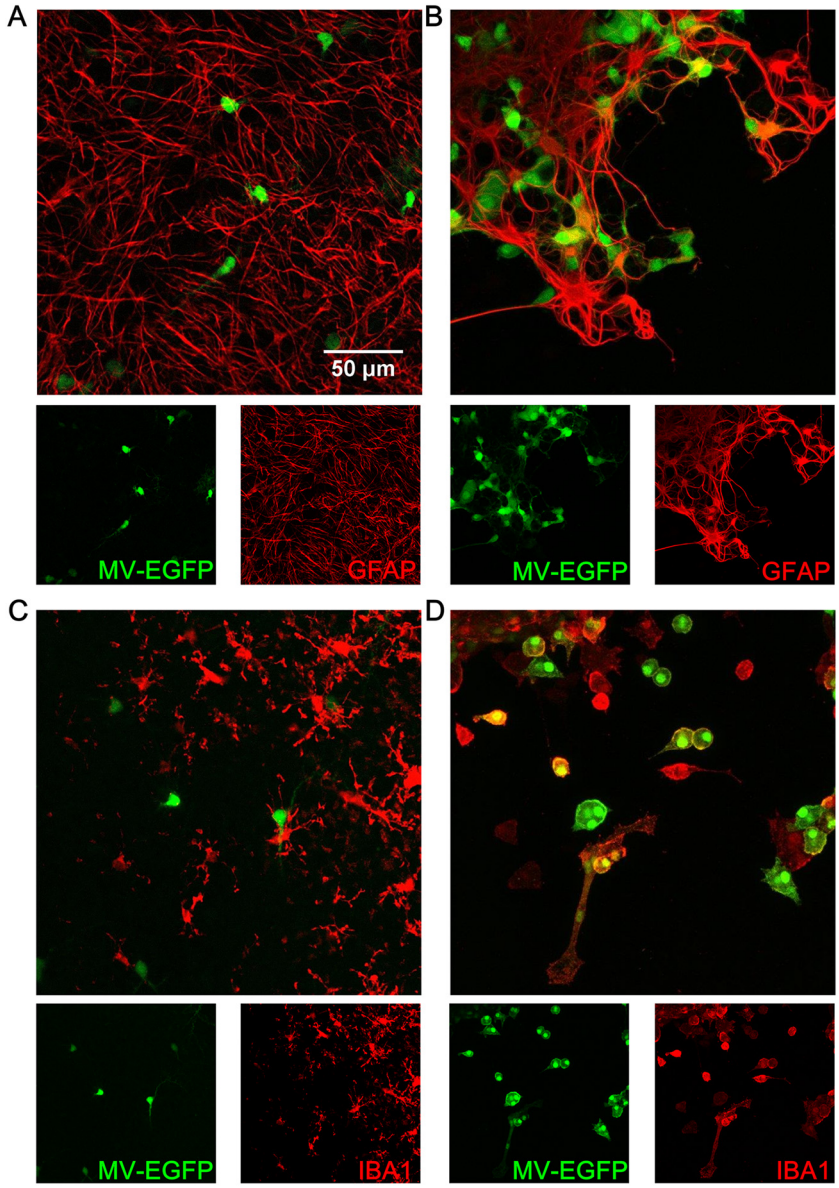

FIG 8 Confocal analysis of cell susceptibility to MeV-EGFP infection in hippocampus slices at day 7 of culture. (A) Astrocytes in a SLAM transgenic mouse. (B) Astrocytes in a SLAM × IFNAR^{KO} transgenic mouse. (C) Microglia in a SLAM transgenic mouse. (D) Microglia in a SLAM × IFNAR^{KO} transgenic mouse. Cell staining (i.e., staining for GFAP for astrocytes and IBA1 for microglia) is represented in red, and EGFP is represented in green.

ple, as observed in Fig. 3C, fewer neurons may be present in SLAM × IFNAR^{KO} explants after a week since their survival seems to be particularly dependent on functional IFN-β signaling (44). Importantly, the acquisition of a limited antiviral state by the SLAM × IFNAR^{KO} tissue over the time course of the culture was not related to any basal IFNAR signaling, as suggested by the accumulation of IFN-β mRNA: the strictly IFN-dependent MX1 gene was not upregulated in SLAM × IFNAR^{KO} OBC, contrary to the findings for SLAM OBC (Fig. 2). The late accumulation of IFN-β mRNA may be related to the absence of direct or indirect negative-feedback IFNAR signaling, such as by IL-1, which is known to prevent an out-of-control response of IFNAR activation (45) but which remains inefficient.

This result indicates that the so-called activated phenotype observed histologically can be fundamentally different in terms of the secretome, leading to totally different

antiviral properties. Indeed, we have shown that the SLAM × IFNAR^{KO} astrogliosis observed here leads to the overexpression of very few secreted factors with very little effect on global infection or cell susceptibility (both after slicing and after infection).

In SLAM OBC, the slicing procedure and culture led to the activation of astrocytes with a specific secreted protein profile, significantly reducing both the susceptibility of the global explant and that of astrocytes and microglia. The reported results are consistent with previously observed patterns of expression, among which several antiviral genes are activated during this response. Among these genes, IFN-γ, which is overexpressed only in SLAM explants, may also play an important role in the diminution of slice susceptibility to infection after several days of culture (46). Possibly, it can directly act on neurons through the extracellular signal-regulated kinase 1/2 (Erk1/2) pathway to block MeV propagation (46, 47). Microglia in OBC seem to be endowed with an IFN-I-dependent intrinsic resistance that limits their permissiveness to MeV infection. Their lower susceptibility to infection seems to correlate with the findings of postmortem analysis of brains from patients who succumbed to MeV subacute sclerosing panencephalitis, in which this cell type only rarely harbors viral antigens. Furthermore, their activation, together with that of astrocytes during astrogliosis, renders the two cell types fully resistant to viral infection via IFN-I signaling (fig. 8). The acquisition of this refractory phenotype to MeV infection after the IFN-I response that occurs during astrogliosis suggests that these cells are particularly suited to recognize and control MeV infection and, consequently, may limit MeV spread through the hippocampus. This may also explain why astrocytes (and, again, microglia) are not systematically found to be positive for MeV antigens in postmortem analyses. Both astrocytes and microglia are the main IFN-I producers in the CNS, and both respond to the activation of IFNAR (48–50). They have been shown to play a critical role in RIG-I-like receptor and IFN-I signaling, governing reactive gliosis and the regulation of innate immune responses after CNS injury in other compartments (51). While part of the loss of slice susceptibility to MeV infection can be directly attributed to the activation of antiviral activity in astrocytes and microglia by secreted IFN-β, possibly via an autocrine pathway, a difference between the SLAM and SLAM × IFNAR^{KO} models may also rely on the production of proinflammatory cytokines, such as IL-1β, that are observed only in the SLAM model: IL-1 is required for astrocytes to be fully functional in the repair of brain lesions (52).

Finally, the infection in SLAM OBC led to a third profile in which all proteins from the uninfected pattern were overexpressed, but with some being significantly more overexpressed. Interestingly, MeV infection at the time of slicing further increases a largely similar set of secreted proteins, but notably, some of them (i.e., IL-8, CXCL2, CCL4) that are generally observed upon the infection of peripheral blood cells by MeV are lacking (53). A few others, such as PDGF-BB and MMP9, already involved in other models of encephalitis and observed only after MeV infection in SLAM OBC, may play a crucial role in the progression to encephalitis (32, 33). Thus, CNS cells seemingly respond to the infection more through a global system involving most of the pathways but in a way different from that in which they respond to the infection observed in peripheral cells, which generally leads to a strong inflammatory antiviral response. Whether the higher production and secretion of cytokines/chemokines in response to an infection could be at the origin of a total loss of the homeostasis in the CNS, potentially leading to encephalitis, remains to be further deciphered.

Conclusion. This work pinpoints several features of differential astrogliosis/inflammatory IFN-I-related responses to slicing of *ex vivo* brain explants. The slicing process reveals a brain cellular heterogeneity with the resistance of astrocytes and microglia to MeV infection through IFNAR signaling, even when viral entry is artificially allowed by the ectopic expression of the human cellular SLAM receptor. While a lower level of expression of an unknown CNS cell entry receptor for MeV may play a role, these observations may at least partially explain the inconstancy of the data concerning the presence of the MeV in astrocytes and microglia in humans in postmortem analysis. To

go further, this study also highlights that while the infection in these two animal models ends in a deadly neurological syndrome, the early events leading to encephalitis in terms of cell susceptibility and the secretome in the CNS parenchyma are significantly different. Determination of whether or not the lower susceptibility of astrocytes and microglia and their ability to control infection through the IFN pathway play a role in the acquisition of mutations observed in the viral sequences isolated from patients dying of MeV encephalitis will require further investigation of viral evolution in the CNS.

Finally, this work could serve as a starting point to compare the impact of IFN-I responses and astrogliosis on brain infection with other neurotropic viruses, notably, for those that use a ubiquitous receptor to invade the CNS. While the use of OBC is expected to be instrumental for such future studies, the choice of the time window in which to perform the viral infection will be a critical parameter to be considered.

MATERIALS AND METHODS

Ethics statement. SLAM tg and SLAM × IFNAR^{KO} mice (males and females, bred at the PBES, ENS-Lyon, animal facility) were handled in strict accordance with good animal practice, as defined by the French national charter on the ethics of animal experimentation. This study was performed according to French ethical committee (CECCAPP) regulations (accreditation CECCAPP_ENS_2014_033).

Brain slice preparation and culture procedure. Brain slices were prepared from SLAM tg and SLAM × IFNAR^{KO} mice (males and females) and maintained in culture as detailed elsewhere (25).

Flow cytometry analysis. After 24 h of infection with MeV IC323-EGFP (2×10^4 PFU/slice), slices were delicately detached and transferred into 0.3 ml of Dulbecco modified Eagle medium (DMEM)-papain (10 mg/ml; Sigma-Aldrich) that had previously been activated at 37°C for 30 min. After 15 min of digestion at 37°C, 0.3 ml of fetal calf serum (FCS) was added to the tube to inactivate the papain and slices were dissociated by flushing. Then, cells were washed using 3 ml of 1× phosphate-buffered saline (PBS) and were spun down (1,800 rpm, 8 min). For extracellular staining, the supernatant was replaced with blocking solution (DMEM without phenol red, 5% FCS) for 30 min at 4°C. Then, the cells were spun down (1,800 rpm, 8 min) and resuspended in 300 μl of DMEM without phenol red, 5% FCS containing antibodies for specific staining: oligodendrocytes with antigalactocerebroside (anti-GALC)-Alexa Fluor 647 (antibody MAB342-AF647; Millipore) diluted 1/100 and microglia with CD11b-allophycocyanin (APC), human and mouse (clone REA592; catalog no. 130-109-286; MACS Miltenyi Biotech), diluted 1/10. After 30 min at 4°C, the cells were washed using 3 ml of 1× PBS and were spun down (1,800 rpm, 8 min). The cells were resuspended with 100 μl of 1× PBS and transferred to cytometry tubes. DAPI (4′,6-diamidino-2-phenylindole) was added to the tubes to assess viability. Cells were acquired on a FACSCanto II flow cytometer (BD Biosciences) or on an ImageStreamX flow cytometer (Merck Millipore) at ×60 magnification. For intracellular staining, cells were resuspended and incubated for 30 min in 1 ml of PBS-containing Live/Dead reagent (1/5,000; Thermo Fisher Scientific) on ice to assess viability. The cells were then washed by adding 10 ml of 1× PBS and were spun down (1,800 rpm, 8 min). The supernatant was removed, and the cells were fixed using 0.3 ml of 2% paraformaldehyde (Sigma-Aldrich). After 20 min, the cells were washed by adding 10 ml of 1× PBS and again spun down (1,800 rpm, 8 min). The supernatant was replaced with 0.3 ml of blocking and permeabilization buffer (1× PBS, 4% fetal bovine serum, 0.3% Triton X-100), and the cells were placed at 4°C for 30 min. After centrifugation (1,800 rpm, 8 min), the supernatant was replaced with blocking and permeabilization buffer containing antibodies for specific staining: neurons were stained with primary anti-beta III tubulin, also known as Tuj1 (rabbit polyclonal; catalog no. ab18207; Abcam), diluted 1/1,000, and astrocytes were stained with astrocytic primary antibody anti-GFAP (glial fibrillary-associated protein; rabbit polyclonal; catalog no. Z0334; Dako) diluted 1/1,000. After 30 min of incubation at 4°C, the cells were washed by adding 10 ml of 1× PBS directly to the tubes and spun down (1,800 rpm, 8 min). The supernatant was replaced with 0.3 ml of blocking and permeabilization buffer containing secondary anti-rabbit immunoglobulin antibodies conjugated with Alexa Fluor 647 (donkey anti-rabbit IgG H+L; catalog no. A-31573; Thermo Fisher Scientific) diluted 1/2,000. After 30 min of incubation at 4°C, the cells were washed by adding 10 ml of 1× PBS directly to the tubes and spun down (1,800 rpm, 8 min). The cells were resuspended in 0.3 ml of 1× PBS in cytometry tubes and acquired on a BD LSR Fortessa flow cytometer (BD Biosciences) or an ImageStreamX flow cytometer (Merck Millipore). Data were analyzed using FlowJo software (TreeStar) for conventional flow cytometry or IDEAS software (Merck Millipore) for image cytometry. To improve the robustness of the analysis, the distribution of the infection is presented as the percentage of each stained population among EGFP-positive cells, while the contribution of each cell type to the overall infection was obtained from the percentage of infected cells in a specific subcellular population.

Evolution of cell composition over 7 days of culture. Slices were prepared from three 7-day-old animals as described below. Slices were transferred at day 0 or 7 into 1 ml of Accutase solution (10 mg/ml; Sigma-Aldrich) that had previously been activated at 37°C for 30 min (1 slice/tube). After 15 min of digestion at 37°C, 1 ml of FCS was added to the tube to inactivate the Accutase and the slices were dissociated by flushing. Then, the cells were washed using 3 ml of 1× PBS and were spun down (1,800 rpm, 8 min). Then, the cells were resuspended on ice in 100 μl of neurobasal medium without

TABLE 2 Primers used in the study

Primer name	Use	Orientation	Sequence (5′–3′)	Amplicon length (bp)	Efficacy	Reference or source
GAPDH	Housekeeping gene	Forward	GCATGGCCTTCCGTGTCC	84	1.98	42
		Reverse	TGTCATCATACTTGGCAGGTTTC			
S100B	Global activation	Forward	TAACTCAGGACCGAGAATC	126	1.98	Designed and validated for this study
		Reverse	GCAAGGAAGATACAACTAACT			
GFAP	Astrocyte proliferation	Forward	GAGACAGAGGAGTGGTAT	103	1.95	Designed and validated for this study
		Reverse	GATAGTCGTTAGCTTCGT			
Alpha interferon	IFN-α mRNA transcription	Forward	CTCTGTGCTTTCCTGATG	90	1.89	42
		Reverse	CCTGAGGTTATGAGTCTG			
Beta interferon	IFN-β mRNA transcription	Forward	TCCACTTGAAGAGCTATTAC	170	1.97	42
		Reverse	CATTCTGAGGCATCAACT			
hSLAM	CD150/human SLAM mRNA transcription	Forward	CGAACCATTACCAGACAA	187	1.95	Designed and validated for this study
		Reverse	GCATAGACTGTGATGGAAT			
MeV nucleoprotein	MeV N mRNA, MeV genome and antigenome	Forward	GTGATCAAAGTGAGAATGAGCT	211	2.13	43
		Reverse	GCTGACCTTCGACTGTCCT			

phenol red–5% FCS containing Live/Dead reagent (1/1,000; Thermo Fisher Scientific) to assess the viability and antibodies for specific staining: oligodendrocytes with anti-GALC-Alexa Fluor 647 (antibody MAB342-AF647; Millipore) diluted 1/100; microglia with anti-CD11b-APC, human and mouse (clone REA592; catalog no. 130-109-286; MACS Miltenyi Biotech), diluted 1/10; neurons with anti-CD24-APC mouse (clone REA743; catalog no. 130-110-689; MACS Miltenyi Biotech) diluted 1/50; and astrocytes with anti-GLAST (ACSA-1)-APC, human, mouse, and rat (clone ASCA-1; catalog no. 130-095-814; MACS Miltenyi Biotech), diluted 1/11. After 30 min on ice, cells were washed using 5 ml of 1× PBS and were spun down (1,800 rpm, 8 min). Cells were resuspended with 100 μl of 1× PBS, transferred to cytometry tubes. and acquired on a BD LSR Fortessa flow cytometer (BD Biosciences).

Immunostaining of brain slices. Immunostaining was performed as described elsewhere (25).

Real-time quantitative PCR. RNA extraction, reverse transcription, and quantitative PCR were performed as previously described (24). The primers used are presented in Table 2. Primers were either designed using Beacon Designer (version 8) software or chosen after validation that their efficacy was close to 100% according to the MIQE checklist (54). All results were normalized to the standard deviation (SD) for GAPDH (glyceraldehyde-3-phosphate dehydrogenase) mRNA, and the calculations were performed as previously described (24).

Protein array. Four hippocampal slices were isolated from SLAM or SLAM × IFNAR^{KO} transgenic mice and harvested on the day of preparation or after 7 days of culture (1 slice per animal and time point). Slices were then triturated and lysed in 1× PBS supplemented with antiprotease cocktail (cOmplete-EDTA; Roche) and 1% Triton X-100 using a syringe and needle (26 gauge). The brain lysates were centrifuged at 10,000 × *g* for 10 min at 4°C, and the supernatants were frozen at −80°C. On the day of the analysis, lysates were thawed and 200 μl was treated following the recommendations of the manufacturer of the Proteome Profiler mouse XL cytokine array kit (catalog no. ARY028; R&D Systems). The proteome kit allows the detection of 111 secreted proteins, including cytokines, chemokines, and growth factors. The results were revealed using a chemiluminescence kit (SuperSignal West Femto Maximum Sensitivity Substrate; catalog no. 34095; Thermo Fisher Scientific). The luminescence signal was acquired with an imaging system (VersaDoc; Bio-Rad). For the normalization of the assay, a bicinchoninic acid protein array kit was used following the recommendations of the manufacturer (catalog no. 23225; Thermo Fisher Scientific).

Infection procedure of brain slices. A recombinant MeV IC323-EGFP (55) stock was diluted in serum-free medium in order to infect cultured slices with 10,000 PFU of MeV. Using a pipette, the diluted viral stock (2 μl) was gently deposited on the top of the slices and the homogeneity of the inoculum was monitored. The plates were incubated at 37°C in a 5% CO_2 humidified atmosphere.

Statistical analysis. The results are presented as the mean + standard deviation (SD). Statistical analyses were performed using the nonparametric Kruskal-Wallis test to assess the variation of mRNA expression with time, and the Mann-Whitney U test was used to compare the number of mRNA copies between SLAM and SLAMSLAM × IFNAR^{KO} samples at a specific time points in GraphPad Prism software (version 5).

For the protein array, statistical calculations and graphical devices were produced using R statistical computing language software (version 3.2.3). To test for the effect of time on the increase in expression between day 0 and day 7, a linear mixed-model regression analysis was used that allows the simultaneous pairing of measurements by animal and by protein in order to properly take into account the interindividual and the interprotein variability. The results showed that this increase was highly significant ($P < 0.001$). Proteins differentially expressed between day 0 and day 7 were determined with the linear model approach from the Bioconductor limma package. Analyses were completed for each mouse strain separately ($n = 4$ mice at each time point). Data were paired by animal, and P values were corrected for multiple testing with the Bonferroni adjustment method. A difference was considered significant when the adjusted P value was <0.05. A two-way ANOVA was performed to test whether the evolution of protein expression over the week of culture was different between SLAM and SLAM × IFNAR^{KO} mice.

ACKNOWLEDGMENTS

This work was supported by a French ANR NITRODEP grant (project ANR-13-PDOC-0010-01; http://www.agence-nationale-recherche.fr) and by PhenoCan Equipex (ANR-11-EQPX-0035 PHENOCAN) and LABEX ECOFECT (ANR-11-LABX-0048) of Lyon University within the program Investissements d'Avenir (ANR-11-IDEX-0007) of the French National Research Agency.

We are grateful to Thibault Andrieu from the AniRA-Cytometry Core Facility (SFR Biosciences, UMS3444/CNRS, US8/INSERM, ENS de Lyon, UCBL, Lyon, France) and the confocal microscopy platform (PLATIM, ENS-Lyon, France) for their assistance. We thank Marion Ferren for excellent technical assistance in the cytometry experiments. We acknowledge Philip Lawrence for English language revision. We also thank the members of the Immunobiology of Viral Infection group (CIRI, Lyon, France) for their help with this study. We are grateful to SERVIER Medical Art, which helped to create Fig. 4A.

REFERENCES

1. Reuter D, Schneider-Schaulies J. 2010. Measles virus infection of the CNS: human disease, animal models, and approaches to therapy. Med Microbiol Immunol 199:261–271. https://doi.org/10.1007/s00430-010-0153-2.
2. Griffin DE. 2014. Measles virus and the nervous system. Handb Clin Neurol 123:577–590. https://doi.org/10.1016/B978-0-444-53488-0.00027-4.
3. Gutierrez J, Issacson RS, Koppel BS. 2010. Subacute sclerosing panencephalitis: an update. Dev Med Child Neurol 52:901–907. https://doi.org/10.1111/j.1469-8749.2010.03717.x.
4. Wilson MR. 2013. Emerging viral infections. Curr Opin Neurol 26:301–306. https://doi.org/10.1097/WCO.0b013e328360dd2b.
5. Patterson JB, Cornu TI, Redwine J, Dales S, Lewicki H, Holz A, Thomas D, Billeter MA, Oldstone MB. 2001. Evidence that the hypermutated M protein of a subacute sclerosing panencephalitis measles virus actively contributes to the chronic progressive CNS disease. Virology 291:215–225. https://doi.org/10.1006/viro.2001.1182.
6. Jurgens EM, Mathieu C, Palermo LM, Hardie D, Horvat B, Moscona A, Porotto M. 2015. Measles fusion machinery is dysregulated in neuropathogenic variants. mBio 6:e02528-14. https://doi.org/10.1128/mBio.02528-14.
7. Leonard VHJ, Sinn PL, Hodge G, Miest T, Devaux P, Oezguen N, Braun W, McCray PB, McChesney MB, Cattaneo R. 2008. Measles virus blind to its epithelial cell receptor remains virulent in rhesus monkeys but cannot cross the airway epithelium and is not shed. J Clin Invest 118:2448–2458. https://doi.org/10.1172/JCI35454.
8. Mühlebach MD, Mateo M, Sinn PL, Prüfer S, Uhlig KM, Leonard VHJ, Navaratnarajah CK, Frenzke M, Wong XX, Sawatsky B, Ramachandran S, McCray PB, Cichutek K, von Messling V, Lopez M, Cattaneo R. 2011. Adherens junction protein nectin-4 is the epithelial receptor for measles virus. Nature 480:530–533. https://doi.org/10.1038/nature10639.
9. Noyce RS, Bondre DG, Ha MN, Lin L-T, Sisson G, Tsao M-S, Richardson CD. 2011. Tumor cell marker PVRL4 (nectin 4) is an epithelial cell receptor for measles virus. PLoS Pathog 7:e1002240. https://doi.org/10.1371/journal.ppat.1002240.
10. Allen IV, McQuaid S, McMahon J, Kirk J, McConnell R. 1996. The significance of measles virus antigen and genome distribution in the CNS in SSPE for mechanisms of viral spread and demyelination. J Neuropathol Exp Neurol 55:471–480. https://doi.org/10.1097/00005072-199604000-00010.
11. Buchanan R, Bonthius DJ. 2012. Measles virus and associated central nervous system sequelae. Semin Pediatr Neurol 19:107–114. https://doi.org/10.1016/j.spen.2012.02.003.
12. Hosoya M. 2006. Measles encephalitis: direct viral invasion or autoimmune-mediated inflammation? Intern Med 45:841–842. https://doi.org/10.2169/internalmedicine.45.0161.
13. Menkes JH, Sarnat HB, Maria BL. 2006. Child neurology. Lippincott Williams & Wilkins, Philadelphia, PA.
14. Bancher C, Leitner H, Jellinger K, Eder H, Setinek U, Fischer P, Wegiel J, Wisniewski HM. 1996. On the relationship between measles virus and Alzheimer neurofibrillary tangles in subacute sclerosing panencephalitis. Neurobiol Aging 17:527–533. https://doi.org/10.1016/0197-4580(96)00069-3.
15. Duprex WP, McQuaid S, Hangartner L, Billeter MA, Rima BK. 1999. Observation of measles virus cell-to-cell spread in astrocytoma cells by using a green fluorescent protein-expressing recombinant virus. J Virol 73:9568–9575.
16. Mesquita R, Castaños-Velez E, Biberfeld P, Troian RM, Siqueira MM. 1998. Measles virus antigen in macrophage/microglial cells and astrocytes of subacute sclerosing panencephalitis. APMIS 106:553–561. https://doi.org/10.1111/j.1699-0463.1998.tb01384.x.
17. Gerlier D, Lyles DS. 2011. Interplay between innate immunity and negative-strand RNA viruses: towards a rational model. Microbiol Mol Biol Rev 75:468–490. https://doi.org/10.1128/MMBR.00007-11.
18. Mrkic B, Odermatt B, Klein MA, Billeter MA, Pavlovic J, Cattaneo R. 2000. Lymphatic dissemination and comparative pathology of recombinant measles viruses in genetically modified mice. J Virol 74:1364–1372. https://doi.org/10.1128/JVI.74.3.1364-1372.2000.
19. Ohno S, Ono N, Seki F, Takeda M, Kura S, Tsuzuki T, Yanagi Y. 2007. Measles virus infection of SLAM (CD150) knockin mice reproduces tropism and immunosuppression in human infection. J Virol 81:1650–1659. https://doi.org/10.1128/JVI.02134-06.
20. Sellin CI, Horvat B. 2009. Current animal models: transgenic animal models for the study of measles pathogenesis. Curr Top Microbiol Immunol 330:111–127.
21. Sellin CI, Davoust N, Guillaume V, Baas D, Belin M-F, Buckland R, Wild TF, Horvat B. 2006. High pathogenicity of wild-type measles virus infection in CD150 (SLAM) transgenic mice. J Virol 80:6420–6429. https://doi.org/10.1128/JVI.00209-06.
22. Mathieu C, Huey D, Jurgens E, Welsch JC, DeVito I, Talekar A, Horvat B, Niewiesk S, Moscona A, Porotto M. 2015. Prevention of measles virus infection by intranasal delivery of fusion inhibitor peptides. J Virol 89:1143–1155. https://doi.org/10.1128/JVI.02417-14.
23. Bloyet L-M, Welsch J, Enchery F, Mathieu C, de Breyne S, Horvat B, Grigorov B, Gerlier D. 2016. HSP90 chaperoning in addition to phosphoprotein required for folding but not for supporting enzymatic activities of measles and Nipah virus L polymerases. J Virol 90:6642–6656. https://doi.org/10.1128/JVI.00602-16.
24. Welsch JC, Talekar A, Mathieu C, Pessi A, Moscona A, Horvat B, Porotto M. 2013. Fatal measles virus infection prevented by brain-penetrant fusion inhibitors. J Virol 87:13785–13794. https://doi.org/10.1128/JVI.02436-13.
25. Welsch JC, Lionnet C, Terzian C, Horvat B, Gerlier D, Mathieu C. 2017. Organotypic brain cultures: a framework for studying CNS infection by neurotropic viruses and screening antiviral drugs. Bio-Protoc 7:e2605.
26. Ludlow M, Duprex WP, Cosby SL, Allen IV, McQuaid S. 2008. Advantages of using recombinant measles viruses expressing a fluorescent reporter gene with vibratome slice technology in experimental measles neuropathogenesis. Neuropathol Appl Neurobiol 34:424–434. https://doi.org/10.1111/j.1365-2990.2007.00900.x.
27. Eng LF, Ghirnikar RS. 1994. GFAP and astrogliosis. Brain Pathol 4:229–237. https://doi.org/10.1111/j.1750-3639.1994.tb00838.x.
28. Fitch MT, Silver J. 2008. CNS injury, glial scars, and inflammation: inhibitory extracellular matrices and regeneration failure. Exp Neurol 209:294–301. https://doi.org/10.1016/j.expneurol.2007.05.014.
29. Little AR, O'Callagha JP. 2001. Astrogliosis in the adult and developing

CNS: is there a role for proinflammatory cytokines? Neurotoxicology 22:607–618. https://doi.org/10.1016/S0161-813X(01)00032-8.
30. Sofroniew MV. 2014. Astrogliosis. Cold Spring Harb Perspect Biol 7:a020420. https://doi.org/10.1101/cshperspect.a020420.
31. Potula R, Dhillion N, Sui Y, Zien CA, Funa K, Pinson D, Mayo MS, Singh DK, Narayan O, Buch S. 2004. Association of platelet-derived growth factor-B chain with simian human immunodeficiency virus encephalitis. Am J Pathol 165:815–824. https://doi.org/10.1016/S0002-9440(10)63344-5.
32. Bethel-Brown C, Yao H, Callen S, Lee YH, Dash PK, Kumar A, Buch S. 2011. HIV-1 Tat-mediated induction of platelet-derived growth factor in astrocytes: role of early growth response gene 1. J Immunol 186:4119–4129. https://doi.org/10.4049/jimmunol.1002235.
33. Ichiyama T, Matsushige T, Siba P, Suarkia D, Takasu T, Miki K, Furukawa S. 2008. Cerebrospinal fluid levels of matrix metalloproteinase-9 and tissue inhibitor of metalloproteinase-1 in subacute sclerosing panencephalitis. J Infect 56:376–380. https://doi.org/10.1016/j.jinf.2008.02.014.
34. Rempe RG, Hartz AMS, Bauer B. 2016. Matrix metalloproteinases in the brain and blood-brain barrier: versatile breakers and makers. J Cereb Blood Flow Metab 36:1481–1507. https://doi.org/10.1177/0271678X16655551.
35. Chen J, Xu W, Chen Y, Xie X, Zhang Y, Ma C, Yang Q, Han Y, Zhu C, Xiong Y, Wu K, Liu F, Liu Y, Wu J. 2017. Matrix metalloproteinase 9 facilitates hepatitis B virus replication through binding with type I interferon (IFN) receptor 1 to repress IFN/JAK/STAT signaling. J Virol 91:e01824-16. https://doi.org/10.1128/JVI.01824-16.
36. O'Donnell LA, Conway S, Rose RW, Nicolas E, Slifker M, Balachandran S, Rall GF. 2012. STAT1-independent control of a neurotropic measles virus challenge in primary neurons and infected mice. J Immunol 188:1915–1923. https://doi.org/10.4049/jimmunol.1101356.
37. Ehrengruber MU, Ehler E, Billeter MA, Naim HY. 2002. Measles virus spreads in rat hippocampal neurons by cell-to-cell contact and in a polarized fashion. J Virol 76:5720–5728. https://doi.org/10.1128/JVI.76.11.5720-5728.2002.
38. Makhortova NR, Askovich P, Patterson CE, Gechman LA, Gerard NP, Rall GF. 2007. Neurokinin-1 enables measles virus trans-synaptic spread in neurons. Virology 362:235–244. https://doi.org/10.1016/j.virol.2007.02.033.
39. Alves L, Khosravi M, Avila M, Ader-Ebert N, Bringolf F, Zurbriggen A, Vandevelde M, Plattet P. 2015. SLAM- and nectin-4-independent noncytolytic spread of canine distemper virus in astrocytes. J Virol 89:5724–5733. https://doi.org/10.1128/JVI.00004-15.
40. Cavanaugh SE, Holmgren AM, Rall GF. 2015. Homeostatic interferon expression in neurons is sufficient for early control of viral infection. J Neuroimmunol 279:11–19. https://doi.org/10.1016/j.jneuroim.2014.12.012.
41. Hofman FM, Hinton DR, Baemayr J, Weil M, Merrill JE. 1991. Lymphokines and immunoregulatory molecules in subacute sclerosing panencephalitis. Clin Immunol Immunopathol 58:331–342. https://doi.org/10.1016/0090-1229(91)90124-S.
42. Manchester M, Eto DS, Oldstone MB. 1999. Characterization of the inflammatory response during acute measles encephalitis in NSE-CD46 transgenic mice. J Neuroimmunol 96:207–217. https://doi.org/10.1016/S0165-5728(99)00036-3.
43. Mrkic B, Pavlovic J, Rülicke T, Volpe P, Buchholz CJ, Hourcade D, Atkinson JP, Aguzzi A, Cattaneo R. 1998. Measles virus spread and pathogenesis in genetically modified mice. J Virol 72:7420–7427.
44. Ejlerskov P, Hultberg JG, Wang J, Carlsson R, Ambjørn M, Kuss M, Liu Y, Porcu G, Kolkova K, Friis Rundsten C, Ruscher K, Pakkenberg B, Goldmann T, Loreth D, Prinz M, Rubinsztein DC, Issazadeh-Navikas S. 2015. Lack of neuronal IFN-β-IFNAR causes Lewy body- and Parkinson's disease-like dementia. Cell 163:324–339. https://doi.org/10.1016/j.cell.2015.08.069.
45. Ivashkiv LB, Donlin LT. 2014. Regulation of type I interferon responses. Nat Rev Immunol 14:36–49. https://doi.org/10.1038/nri3581.
46. Patterson CE, Lawrence DMP, Echols LA, Rall GF. 2002. Immune-mediated protection from measles virus-induced central nervous system disease is noncytolytic and gamma interferon dependent. J Virol 76:4497–4506. https://doi.org/10.1128/JVI.76.9.4497-4506.2002.
47. O'Donnell LA, Henkins KM, Kulkarni A, Matullo CM, Balachandran S, Pattisapu AK, Rall GF. 2015. Interferon gamma induces protective non-canonical signaling pathways in primary neurons. J Neurochem 135:309–322. https://doi.org/10.1111/jnc.13250.
48. Blank T, Prinz M. 2017. Type I interferon pathway in CNS homeostasis and neurological disorders. Glia 65:1397–1406. https://doi.org/10.1002/glia.23154.
49. Tedeschi B, Barrett JN, Keane RW. 1986. Astrocytes produce interferon that enhances the expression of H-2 antigens on a subpopulation of brain cells. J Cell Biol 102:2244–2253. https://doi.org/10.1083/jcb.102.6.2244.
50. Pfefferkorn C, Kallfass C, Lienenklaus S, Spanier J, Kalinke U, Rieder M, Conzelmann K-K, Michiels T, Staeheli P. 2016. Abortively infected astrocytes appear to represent the main source of interferon beta in the virus-infected brain. J Virol 90:2031–2038. https://doi.org/10.1128/JVI.02979-15.
51. de Rivero Vaccari JP, Minkiewicz J, Wang X, de Rivero Vaccari JC, German R, Marcillo AE, Dietrich WD, Keane RW. 2012. Astrogliosis involves activation of Rig-like signaling in the innate immune response after spinal cord injury. Glia 60:414–421. https://doi.org/10.1002/glia.22275.
52. Herx LM, Yong VW. 2001. Interleukin-1 beta is required for the early evolution of reactive astrogliosis following CNS lesion. J Neuropathol Exp Neurol 60:961–971. https://doi.org/10.1093/jnen/60.10.961.
53. Zilliox MJ, Moss WJ, Griffin DE. 2007. Gene expression changes in peripheral blood mononuclear cells during measles virus infection. Clin Vaccine Immunol 14:918–923. https://doi.org/10.1128/CVI.00031-07.
54. Bustin SA, Benes V, Garson JA, Hellemans J, Huggett J, Kubista M, Mueller R, Nolan T, Pfaffl MW, Shipley GL, Vandesompele J, Wittwer CT. 2009. The MIQE guidelines: minimum information for publication of quantitative real-time PCR experiments. Clin Chem 55:611–622. https://doi.org/10.1373/clinchem.2008.112797.
55. Hashimoto K, Ono N, Tatsuo H, Minagawa H, Takeda M, Takeuchi K, Yanagi Y. 2002. SLAM (CD150)-independent measles virus entry as revealed by recombinant virus expressing green fluorescent protein. J Virol 76:6743–6749. https://doi.org/10.1128/JVI.76.13.6743-6749.2002.